Enhanced Isolation of a Closely-spaced Four-element MIMO Antenna System Using Metamaterial Mushroom

Guohua Zhai, *Member, IEEE,* Zhi Ning Chen, *Fellow, IEEE,* Xianming Qing, *Senior Member, IEEE*

***Abstract*— A double-layer mushroom structure is proposed to enhance the inter-element isolation of a four-element antenna system, wherein four closely positioned substrate integrated cavity-backed slot (SICBS) antenna elements are configured for multiple-input multiple-output (MIMO) applications. A wall with a double-layer mushroom structure is positioned in between the four antenna elements. An antenna prototype with a ground plane size of 0.96 λ_0 × 0.96 λ_0 (λ_0 is the free space-wavelength at 2.4 GHz) demonstrates an enhanced inter-element isolation of 16 dB for parallel directed antenna element pairs, while the isolation of the orthogonally directed antenna element pairs remains unchanged over the operating bandwidth (|S_{11}|<-10 dB) of 2.396 GHz–2.45 GHz. With the enhanced isolation larger than 42 dB between each antenna element pair, the envelope correlation coefficient (ECC) is lower than 0.02 across the operating bandwidth. The simulated and measured results validate the good MIMO diversity performance of the proposed antenna system.**

***Index Terms*—Multiple-input multiple-output (MIMO), MIMO antenna, metamaterial, substrate integrated waveguide (SIW), cavity-backed slot antenna (CBS), isolation, mushroom, mutual coupling, envelope correlation coefficient.**

I. Introduction

With further requirements of larger channel capacity in wireless communication systems, multiple-input multiple-output (MIMO) technology has been integrated into the fourth generation long term evolution (4G LTE) standard to overcome the shadowing and fading phenomena in multipath environments [1]. A low envelope correlation coefficient (ECC) benefits the enhancement of the high channel capacity of MIMO systems, which is directly affected by the impedance matching and the isolation of the multi-element antennas in the MIMO systems [2], [3]. The poor isolation degrades the ECC, reduces the radiation efficiency, and abates the channel capacity [4]. Furthermore, the channel capacity is significantly enhanced with the increasing order in an $N \times N$ MIMO system [5], namely, the system capacity can be enhanced by using more antenna elements. However, with the limited size, the close proximity of the multiple antenna elements leads to a lower isolation. Therefore, the isolation between antenna elements is one of the key issues for the design of the MIMO systems.

A number of techniques have been reported to enhance the isolation of two antenna elements, they can be classified as the introduction of offsetting branches [6], [7], the usage of modified ground [8], the utilization of metamaterials [9–12], as well as the adoption of decoupling networks [13]. Regarding the four-element antenna system, the reported techniques include the utilization of decoupling networks [14–17], optimization of antenna system configurations [18], [19], introduction of metamaterial structures including split ring resonators (SRRs) [20–22] and planar mushroom [23], as well as any combination of the decoupled methods mentioned above [24], [25]. However, with the strong industrial requirement of higher data-rata transmission and larger channel capacity for forthcoming wireless communication systems (for example IEEE 802.11n), industry applications require an ultra high inter-element isolation, for example larger than 40 dB, simultaneously for all four antenna elements in a closely spaced MIMO antenna system to enhance their diversity performance at a system level. The existing configuration of four-element MIMO antenna systems is suffering from the low isolation between the parallel directed antenna elements pair with the same polarization.

In this paper, a compact double-layer mushroom structure is proposed to enhance the inter-element isolation of the closely spaced four-element MIMO antenna system. A wall with the double-layer mushroom structure is symmetrically positioned in between the substrate integrated cavity-backed slot (SICBS) antenna elements, which blocks and absorbs the space-field/near-field from the antenna elements and thus enhances the inter-element isolation significantly. Compared to the planar mushroom structures mainly for suppressing the surface-wave coupling of four-element MIMO antennas [23], the proposed double-layer mushroom wall not only controls the space-field and near-field of the MIMO antenna but also reduces its transverse size.

This paper is arranged as follows. In Section II, the inter-element coupling of the four-element antenna system with different configurations is discussed. Section III presents the methodology of the double-layer mushroom wall and study of its effects on the inter-element isolation of the four-element antenna system. Section IV shows the simulated and measured

Manuscript received ?, 2014. This work was partially supported by the Agency for Science, Technology, and Research (A*STAR), Singapore, Metamaterials Program under Grant #0921540097 and Economic Development Board (EDB), Singapore, under the office for space technology and industry (OSTIn) Space Industry Alignment Grant ("SIAG") S14-1139-IAF OSTIn-SIAG.

G. H. Zhai was with the School of Information and Science Technology, East China Normal University, Shanghai 200241(e-mail: ghzhai@ee.ecnu.edu.cn). He is now with the Institute for Infocomm Research, A*STAR, Singapore 138632 (e-mail: zhaigh@ i2r. a-star.edu.sg).

Z. N. Chen, and X. Qing are with the Institute for Infocomm Research, A*STAR, Singapore 138632 (e-mail: Chenzn@i2r.a-star.edu.sg, qingxm@i2r .a-star.edu.sg).

Z. N. Chen is also with the Department of Electrical and Computer Engineering, National University of Singapore, Singapore 117583 (e-mail: eleczn@nus.edu.sg).

results. A summary is presented in Section V. The antenna system is designed and optimized using CST Microwave Studio [26].

II. FOUR-ELEMENT SICBS ANTENNA SYSTEM

A. Probe fed antenna element

The design principle of the SICBS antenna element fed by a co-planar waveguide (CPW) has been studied in detail [27]. In this work, in order to reduce the size, the antenna element is fed by a probe as shown in Fig. 1, where Rogers RO4003C (ε_r=3.5, tanδ= 0.0027) with a thickness of h_0 is used. The geometrical parameters of the antenna element are: b=80 mm, a_1=21.58 mm, a_2=25.53 mm, a_3=4.63 mm, a=51.06 mm, l=47.6 mm, w=8 mm, d=0.5 mm, p=0.76 mm, h_0=1.524 mm. The simulated $|S_{11}|$ and gain of the antenna element is shown in Fig. 2, which exhibits a bandwidth ($|S_{11}|$<-10 dB) of 2.4 GHz–2.435 GHz with the maximum realized gain of 5.1 dBi at 2.42 GHz.

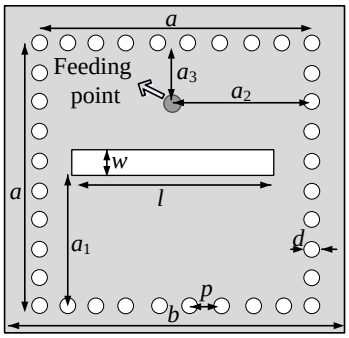

Fig. 1. The geometry of the probe fed SICBS antenna element.

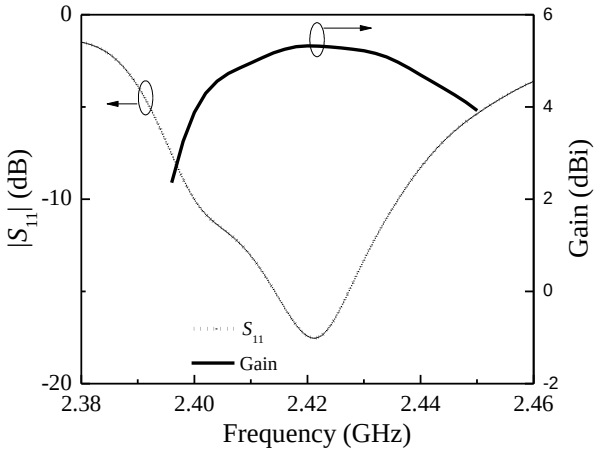

Fig. 2. Simulated $|S_{11}|$ and gain of the SICBS antenna element.

B. Isolation between two antenna elements

Fig. 3 exhibits the six configurations of the antenna pair with two identical antenna elements for inter-element mutual coupling study, where the center-to-center spacing between the antenna elements, g, is kept unchanged. The first three configurations are defined as below,

- Case 1.1, parallel directed antenna element pair (side-to-side)
- Case 2.1, parallel directed antenna element pair (end-to-end)
- Case 3.1, orthogonally directed antenna element pair (side-to-end)

Removing the substrate and metallic layer between the antenna elements, three more configurations are defined as follows,

- Case 1.2, parallel directed antenna element pair (side-to-side)
- Case 2.2, parallel directed antenna element pair (end-to-end)
- Case 3.2, orthogonally directed antenna element pair (side-to-end)

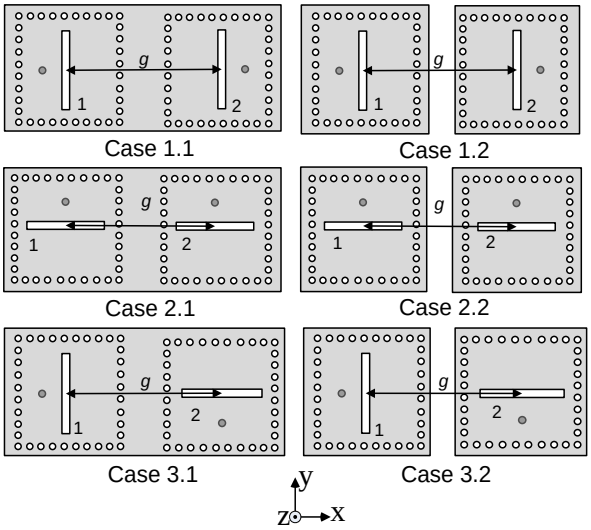

Fig. 3. The configurations of the antenna element pair.

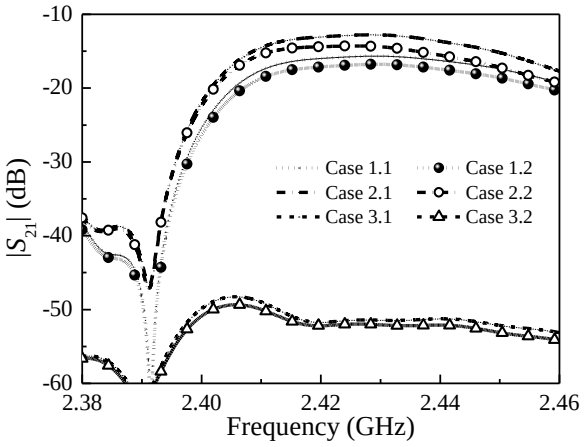

Fig. 4. The isolation of the antenna element pairs (g=54 mm, 0.44 λ_0 @2.42 GHz).

Fig. 4 shows the simulated $|S_{21}|$ of the six scenarios with the same spacing, g=54 mm over the frequency band of 2.38 GHz –2.46 GHz. Fig. 5 exhibits the effects of g on the isolation at the center frequency of 2.42 GHz. It can be seen that with the increasing g up to 63 mm (0.51 λ_0), the isolation of the side-to-side antenna element pair is larger than that of the end-to-end one. However, as g keeps increasing, on the contrary, the isolation of the end-to-end antenna element pair is larger than that of the side-to-side one. Meanwhile, the isolation of the side-to-end antenna element pair is reduced by 25 dB at the

same spacing compared to both the side-to-side and end-to-end cases.

The near-field patterns of Case 1.1 and Case 2.1 (z = 7 mm) are shown in Fig 6. Because of the small distance between the two antenna elements, the adjacent ends of the slot pair of Case 2.1 is more tightly coupled than that of Case 1.1. However, the side-to-side coupling is dominant with the increasing distance between the antenna pair, so the isolation of the antenna element pair of Case 2.1 is larger than that of Case 1.1 when the distance exceeds 0.51 λ_0.

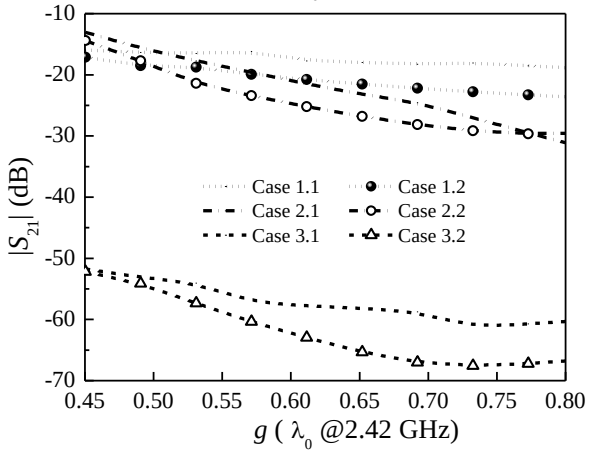

Fig. 5. The effects of g on the isolation of the two antenna elements.

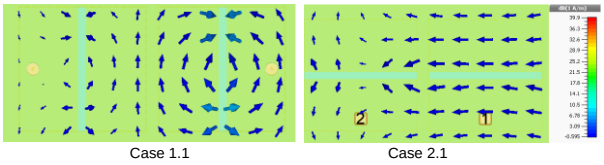

Fig. 6. The H-Field distributions of Case1.1 and Case 2.1 (z = 7 mm, Antenna Element1 is excited @ 2.42 GHz).

For the cases of removing the substrate and metallic layer between two antenna elements, the maximum enhancement of the isolation is 5 dB for both Case 1.1 and Case 2.1, while the maximum one is 8 dB for Case 3.1. Therefore, with the increasing distance, the removal of the substrate and the metallic layer can improve the isolation between two antenna elements. But it has slight effects on the isolation when the distance between the antenna elements is less than 0.5 λ_0, it suggests that the surface wave is not the major factor contributing to the closely-spaced mutual coupling of the antenna elements.

C. Isolation of the four-element SICBS antenna system

The four-element antenna system is shown in Fig.7, where the adjacent antenna elements are orthogonally positioned (side-to-end) and the antenna elements along the diagonal line are parallel directed (side-to-side). It is found that the change of the relative distance between each antenna element has a slight effect on the operating impedance bandwidth of 2.4 GHz–2.44 GHz.

Maintaining g_2, g_3, g_4 unchanged, the influence of the parameter g_1 on the inter-element isolation is studied. When g_1 varies, $|S_{21}|=|S_{43}|$ and $|S_{32}|=|S_{41}|$ are observed. Remaining the distance between Ant. 2 and Ant. 4, the variation of $|S_{42}|$ against g_1 would be negligible, which is verified in Fig. 8. Therefore, as increasing the separation of Ant. 1 and Ant. 3, both $|S_{41}|$ and $|S_{31}|$ decrease because of the larger distance between the antenna elements, and $|S_{21}|$ increases because of the higher cross polarization.

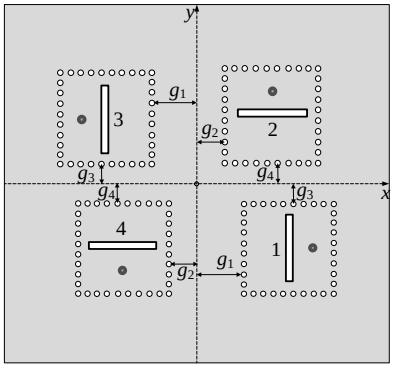

Fig. 7. The geometry of the four-element SICBS antenna system.

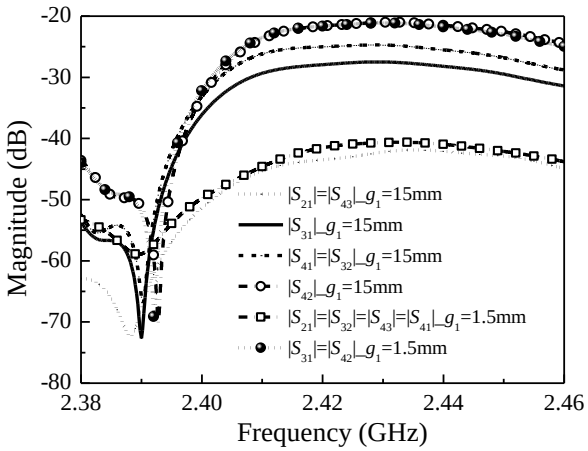

Fig. 8. The isolation of the four-element SICBS antennas with the variation of g_1 (g_2= g_3= g_4=1.5 mm, 0.012 λ_0 @2.42 GHz).

In order to simplify the design and reduce the total size of the four-element antenna system, symmetrically distributed antenna system with the same edge-to-edge distance between adjacent elements is adopted in this work, namely, g_1=g_2=g_3=g_4. The isolation between the parallel positioned adjacent element pairs (Ant.1/Ant.3, Ant.2/Ant.4) is the same, $|S_{31}|=|S_{42}|$. For the orthogonally positioned antenna pairs (Ant.1/Ant.2, Ant.2/ Ant.3, Ant.3/Ant.4, Ant.4/Ant.1), $|S_{21}|=|S_{32}|=|S_{43}|=|S_{41}|$. As shown in Fig. 8, when g_1=g_2=g_3=g_4=1.5 mm, it is observed that the orthogonally positioned antenna pairs achieve the lower inter-element isolation of $|S_{21}|=|S_{32}|=|S_{43}|=|S_{41}|=|S_{31}|$<-40dB while the parallel positioned element pairs exhibit higher inter-element isolation of about 20 dB ($|S_{31}|=|S_{42}|\cong$ -20 dB) within the operating bandwidth. For brevity, only $|S_{11}|$, $|S_{21}|$ and $|S_{31}|$ are presented in the following discussion.

III. ISOLATION ENHANCEMENT USING MUSHROOM WALL

A. Four-element antenna system using mushroom wall

An orthogonally distributed four-element antenna system with the double-layer mushroom wall is shown in Fig. 9,

wherein four pieces of double-layer mushroom walls are symmetrically crossed on top of the antenna elements with a ground plane size of $W_m \times W_m$. The elements are symmetrically arranged at an identical center-to-center distance of g, and separately fed by the coaxial probes, respectively.

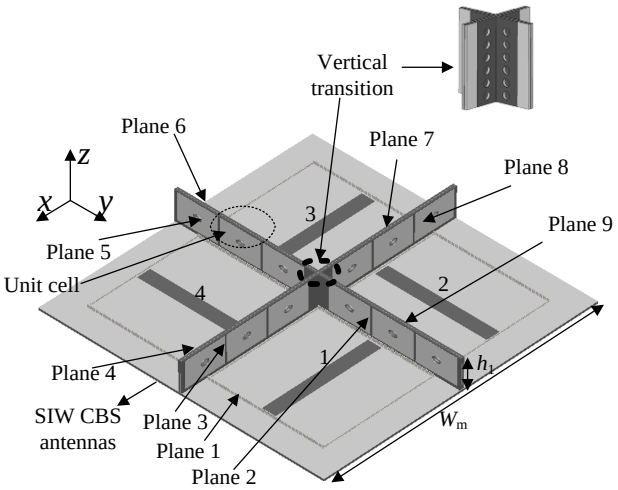

Fig. 9. The geometry of the four-element SICBS antenna system with double-layer mushroom wall.

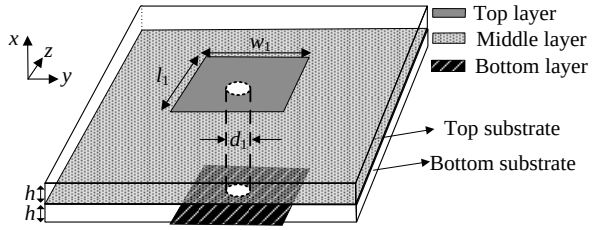

Fig. 10. The geometry of a double-layer mushroom cell.

The mushroom structure features band-gap characteristics, which has been first studied in [28]. In this paper, a double-layer mushroom structure is proposed. As exhibited in Fig. 10, the double-layer mushroom cell is with a two-layer substrate both with a thickness of h, two identical patches with the size of $w_1 \times l_1$ are symmetrically etched on the top layer of the upper substrate and bottom layer of the bottom substrate, respectively. A ground is sandwiched in between and through vias with a diameter of d_1 is utilized to connect the patches to the ground respectively. The mushroom cells are two-dimensionally distributed with a period p_1 along both the y- and z-axes. The numbers of the mushroom cell along y- and z-axes directions are N_y and N_z, respectively. It should be noted that N_y is determined by the operating wavelength and the overall size of the array. N_z can be selected to satisfy specific application requirements of the isolation.

In order to study the mechanism of mutual coupling suppression, the surface-wave band-gap characteristics of the ideal double-layer mushroom structure is analyzed with a patch size of 17.5 × 17.5 mm^2, via radius of 0.76 mm and periodic spacing of 18.2 mm, where a two-layer substrate of Rogers RO4003C with h=0.813 mm, ε_r=3.55, tanδ=0.0027 is used. The simulated results are illustrated in Fig. 11. The TM_0 mode stops at about 2.4 GHz while the TE_1 band begins at about 2.8 GHz. The TM_1 mode starts around 3.2 GHz. A surface-wave forbidden band of 2.4 GHz–2.8 GHz is achieved for the double-layer mushroom.

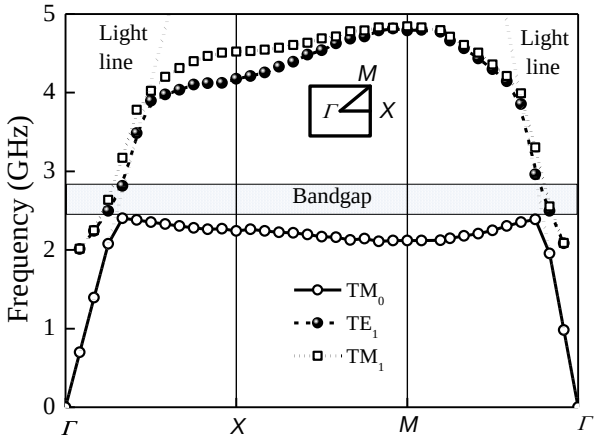

Fig. 11. Surface wave band gap of the double-layer mushroom (achieved from simulation software ANSYS HFSS [29]).

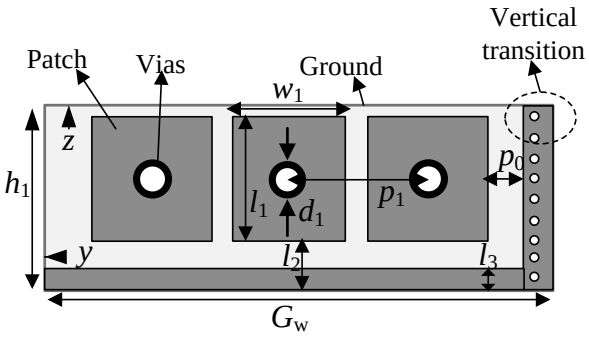

Fig. 12. The geometry of a piece of double-layer mushroom wall.

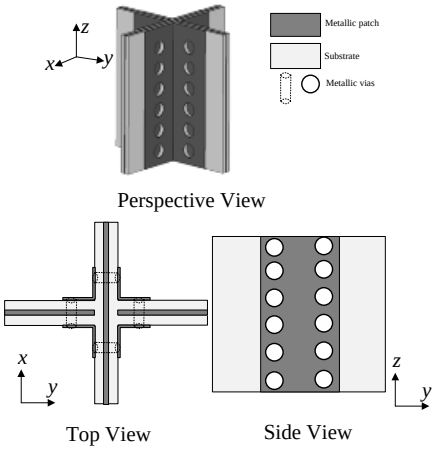

Fig. 13. The geometry of the vertical transition.

Considering the center operating frequency of 2.42 GHz and the height of the antenna system, the mushroom wall with one row and three column (1 × 3) mushroom cells is selected as sketched in Fig 12. Meanwhile, the isolation between the antenna elements is sensitive to the height of the double-layer mushroom above the top of the antenna, l_2. Moreover, in order to electrically connect the middle layer of the mushroom wall

with the ground of the antenna elements, a slit of the top-layer substrate with a width of l_3 is removed to bare the sandwiched metal layer for convenient soldering it with the ground plane of the antenna elements.

Furthermore, to construct the crossed mushroom walls, four rows of metallic vias are implemented to connect the ground of the mushroom wall together. This structure serves as a vertical transition as shown in Fig. 13.

In the following discussion, the PCBs of the SIW antenna system and mushroom wall are Rogers RO4003C with ε_r of 3.38, tanδ of 0.0023, and thickness of h_0=1.524 mm, h=0.813 mm. The parameter of l_3 is kept 1 mm.

B. Optimization and design principle

As shown in Fig. 12, the grounded vertical transition and strip are positioned closely to the double-layer mushroom structures. Such loading structures have larger influences on the band-gap of the mushroom structure, especially for the configuration with less unit cells. The effects of l_2 and p_0 on the isolation between antenna elements are focused on and shown in Fig.14 and Fig. 15, respectively. The impedance bandwidth ($|S_{11}|$ <-10dB) is from 2.4 GHz to 2.44 GHz.

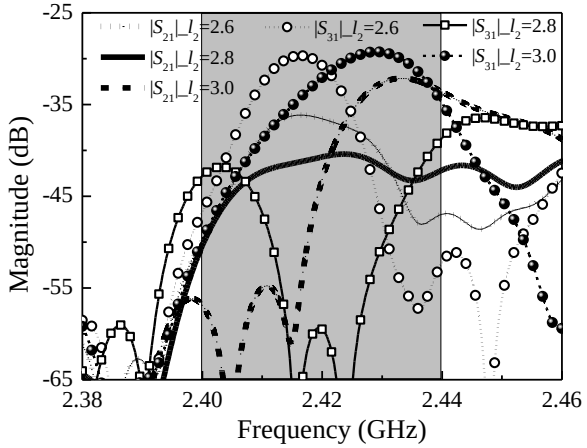

Fig. 14. The effects of l_2 on the isolation between the antenna elements (g=53, p_0=2.7, p_1=18.06, l_1=17.4, d_1=1.52, w_1=17.3, W_m= 11, G_w=59, h_1=20.8. Unit: mm).

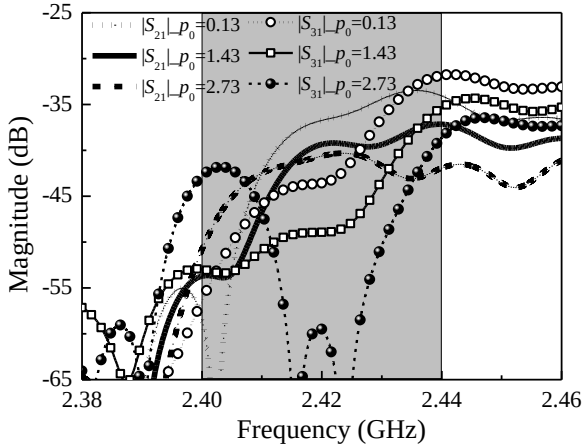

(a) $|S_{21}|$

Fig. 15. The effect of p_0 on the isolation between the antenna elements (g=53, l_2=2.8, p_1=18.06, l_1=17.4, d_1=1.52, w_1=17.3, W_m= 111, G_w=59, h_1=20.8. Unit: mm).

When the field radiated from Ant. 1 is coupled to Ant. 2, the TM mode surface wave propagates along the z-direction crossing over Plane 2 to Plane 9. Therefore, the mushroom structure is moved upwards with the increase of l_2, and thus the surface wave at lower frequencies band would be effectively suppressed by the mushroom structure. In addition, the TE mode surface waves excited by Ant. 1 propagate along the y-axis of the Plane 2 or the x-axis of the Plane 3 to couple the other antennas; they are reflected by the metallic vias of the vertical transition. Thus, with the increase of p_0, the bandgap shifts upwards to the higher frequencies because of the reducing capacitance introduced by the metallic vias of the vertical transition as shown in Fig. 15.

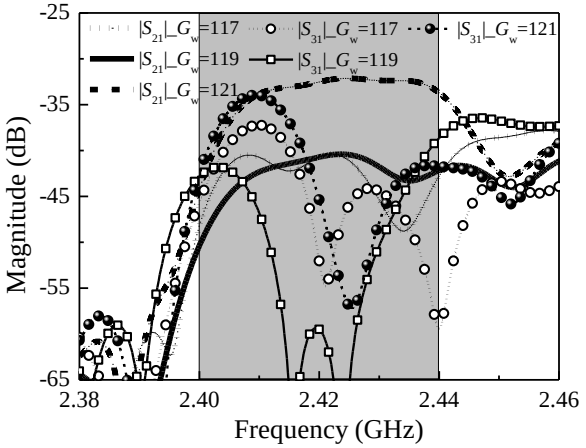

Fig. 16. The effect of G_w on the isolation between the antenna elements (g=53, l_2=2.8, p_0=2.73, p_1=18.06, l_1=17.4, d_1=1.52, w_1=17.3, W_m= 111, h_1=20.8. Unit: mm).

The influence of the length of the mushroom wall with the fixed W_m of 111 mm is exhibited in Fig. 16. It can be observed that the increasing G_m changes the isolation between each antenna element because of the diffraction field.

Regarding the design guideline, the orthogonally distributed compact four-element SICBS antenna system without mushroom structure is designed and optimized first. Next, the double-layer mushroom cell is designed by considering the band-gap characteristics. Then, the four-element antenna system with the double-layer mushroom is optimized to achieve the maximum isolation as desired. The detailed dimensions of the optimized antenna system with mushroom wall as shown in Figs. 1, 9 and 10 are: a_1=22.15 mm, a_2=25 mm, a_3=5.15 mm, a=50.2 mm, w=6.7 mm, l=48.7 mm, d=0.5 mm, p=0.76 mm, g=53 mm, p_0=1.63 mm, p_1=18.06 mm, w_1=17.3 mm, l_1=17.39 mm, l_2=2.75 mm, l_3=1 mm, d_1=1.52 mm, h=0.813 mm, h_1=20.8 mm, W_m=113 mm, and G_w=59.5mm.

C. Comparison of the antenna system with/without mushroom wall

The antenna system with/without a metal wall, perfect magnetic conductor (PMC) wall as well as single-layer mushroom (wherein the patches are printed on Planes 3, 5, 7, and 9, and the metallic ground are printed on Planes 2, 4, 6, and 8) are simulated for comparison. The height and length of the single-layer mushroom, metal wall and PMC wall are with the same as those of the double-layer mushroom.

Keeping the optimized parameters of the four-element MIMO antenna system with the double-layer mushroom unchanged shown above, the reflection coefficients of the antenna system with the walls are shown in Fig. 17. It can be observed that the types of the walls show a significant effect on the impedance matching of the antenna. The parameters of a_1 and a_3 of the antenna system can be tuned for impedance matching.

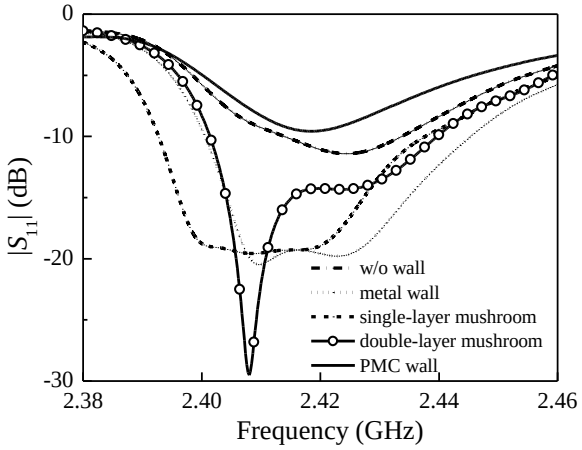

Fig. 17. The reflection coefficient of different walls with the parameters same to double-layer mushroom wall.

The simulated isolation of the four-element antenna system with/without the walls is illustrated in Fig. 18. Compared to the double-layer mushroom wall, the other two walls affect the return loss response of the antenna system. The parameters of a_1 and a_3 are tuned for impedance matching ($|S_{11}|$<−10 dB). Meanwhile, for fair comparison, the single-layer mushroom structure is also optimized for the lowest mutual coupling of the antenna system across the operating range from 2.4 GHz to 2.44 GHz.

Without any wall, the $|S_{21}|$ varies from -42 dB to -39 dB because the antenna elements are orthogonally positioned but $|S_{31}|$ degrades from -37 dB to -25.5 dB within the operating band because Ants. 1 and 3 are positioned in parallel. Loaded with the PMC wall, the isolation between the antenna elements along the horizontal and vertical lines is less than -31 dB, while the one along the parallel lines is less than -41 dB. With the metal wall, the $|S_{21}|$ is less than -39 dB and $|S_{31}|$ is less than -42 dB. Using the single-layer mushroom wall, the $|S_{21}|$ is less than -39 dB from 2.4 GHz to 2.435 GHz, and less than -36 dB from 2.435 GHz–2.44 GHz, and the $|S_{31}|$ is less than -37.5 dB within the band of 2.4 GHz–2.44 GHz. More importantly, by adopting the double-layer mushroom, both $|S_{21}|$ and $|S_{31}|$ are less than -41 within the whole operating band of 2.4 GHz–2.44 GHz. In particular, owing to the band-gap property of the double-layer mushroom, $|S_{31}|$ is less than -60 dB over the range from 2.415 GHz to 2.426 GHz.

Due to the bandgap feature of the mushroom structure, at the center frequency of 2.42 GHz, the isolation of the four-element antenna system can be enhanced by 3.5/22 dB for the orthogonal/parallel directed antenna element pairs. In addition, compared to the antenna systems with the same height metal wall, isolation enhancements of 3/39 dB for the orthogonal/parallel directed antenna element pairs are achieved by using double-layer mushroom wall. Meanwhile, compared to the four-element MIMO antenna system with a single-layer mushroom wall, both the envelopes of the $|S_{21}|$ and $|S_{31}|$ of that with a double-layer wall can be further enhanced by 5 dB within the whole operating impedance band. Thus, the double-layer mushroom can be used to enhance the isolation to meet the system requirement of high isolations between each element.

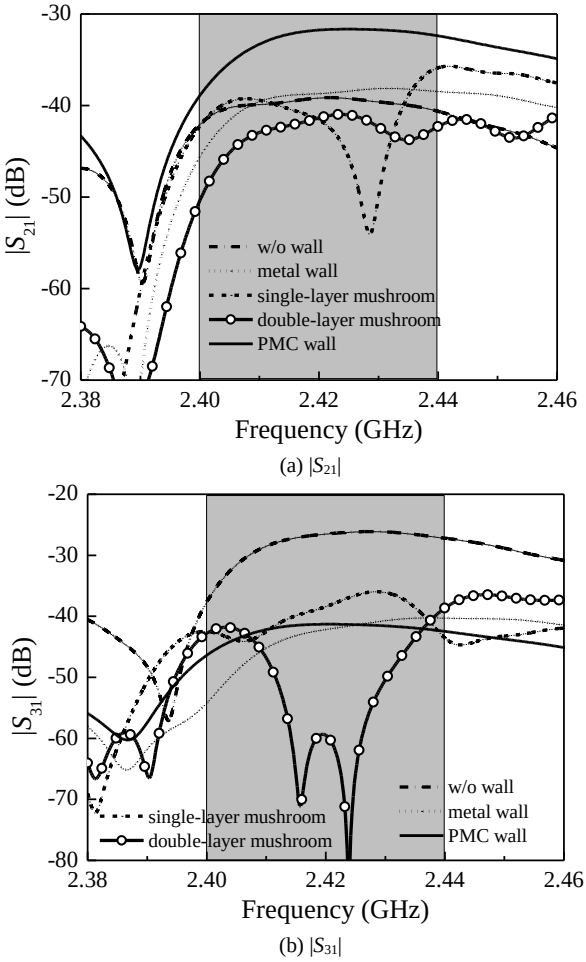

Fig. 18. The comparison of the simulated *S*-parameters of the four-element antenna system with metal wall, and with/without mushroom wall as well as PMC wall.

D. Field distributions

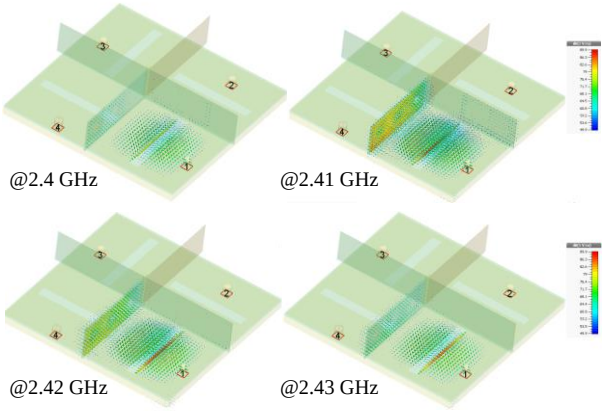

Fig. 19. The simulated *E*-field distribution (excited by Antenna 1).

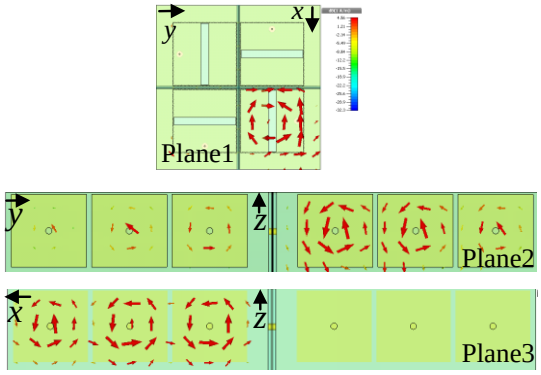

Fig. 20. The simulated *H*-field distribution along the Plane1, 2, and 3 (excited by Antenna 1 at 2.42 GHz).

The three-dimensional *E*-field distribution at 2.4 GHz, 2.41 GHz, 2.42 GHz, and 2.43 GHz are shown in Fig. 19. The two-dimensional *H*-field distribution along Planes 1, 2 and 3 at 2.42 GHz are exhibited in Fig. 20. It is observed that when Antenna 1 is excited, the electromagnetic energy is almost trapped in the closest space (x>0 and y>0) of the mushroom wall, and the coupled wave to other antenna elements is negligible. Meanwhile, negligible amount of energy wave is leaking to other planes (x<0 or y<0). The results validates that the mushroom wall is an effective way to improve the isolation between antenna elements.

IV. FABRICATION AND MEASUREMENT

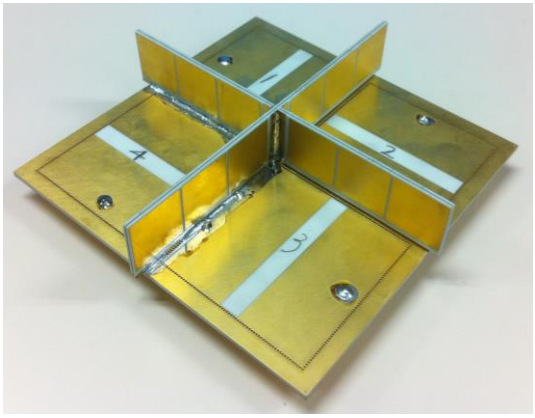

Fig. 21. The photo of the antenna prototype.

The antenna is prototyped and measured. Two pieces of 0.813 mm-thick RO4003C board glued together by a 0.202 mm-thick RO4450B (ε_r=3.54, tanδ=0.004) Prepreg sheet form the 1.83 mm-thick mushroom wall which includes 1 × 3 mushroom cells. The four-element SICBS antenna system is fabricated on a single layer substrate Rogers RO4003C with a thickness of 1.5 mm. The photo of the antenna prototype with an overall size of $0.96\lambda_0 \times 0.96\lambda_0 \times 0.18\lambda_0$ (119 × 119× 22.5 mm^3) is shown in Fig. 21.

The measured and simulated *S*-parameters of the antenna prototype are shown in the Fig. 22. The measured $|S_{11}|$ is less than -10 dB from 2.396 GHz to 2.45 GHz in a good agreement with the simulated results.

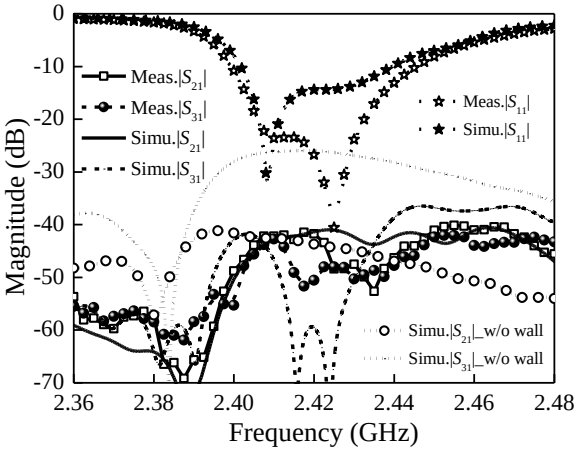

Fig. 22. Measured *S*-parameters of the four-element antenna system.

Both $|S_{21}|$ and $|S_{31}|$ are less than -42 dB over the operating band of 2.396 GHz–2.45 GHz. Furthermore, both the $|S_{21}|$ and $|S_{31}|$ are less than -48 dB from 2.425 GHz to 2.445 GHz. Therefore, keeping the $|S_{21}|$ hardly changed, $|S_{31}|$ is enhanced up to 16 dB crossing the whole band, and up to 22 dB within the band of 2.415 GHz–2.445 GHz, which suggests that the mushroom has significantly enhanced the isolation between antenna elements.

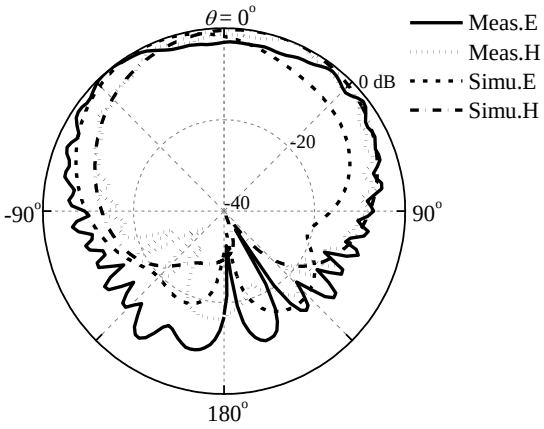

Fig. 23. Measured and simulated radiation patterns of the four-element antenna system (Antenna 1@2.42 GHz).

The simulated and measured far-field radiation patterns in both the *E*- and *H*-planes of the Ant. 1 at 2.42 GHz are shown in Fig. 23. The little difference between the simulation and measurement may come from the fabrication errors. The beam squinting is caused by the reflection from the mushroom wall, and the deflections of *E*-plane and *H*-plane pattern are about ±26° from the bore-sight direction, respectively. It can be observed that within the operating band of 2.396 GHz–2.45 GHz, the front-to-back ratio is larger than 25 dB, and the cross-polarization level is less than -15 dB. For the four-element SICBS antenna system with mushroom wall, the measured maximum realized gain of 4 dBi is achieved at 2.42 GHz, which is decreased by 0.5 dB compared to that without any wall.

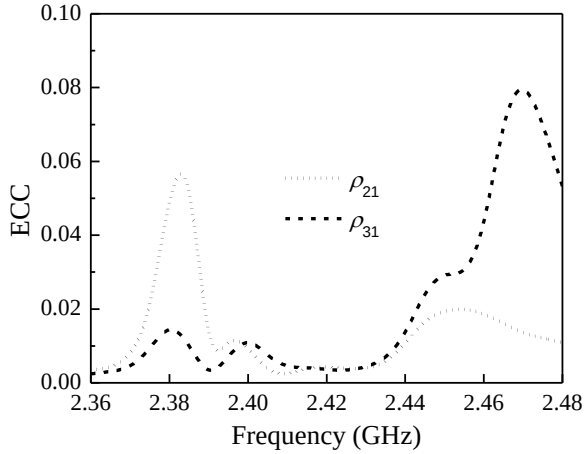

Fig. 24. Calculated ECC of the four-element antenna system.

Because of the good agreement between the simulated and measured patterns, the enveloped correlation co-efficient (ECC) (ρ_{ij}) among the four-element antenna system with the mushroom wall can be calculated using (1) with the simulated three-dimensional far-fields [2] as shown in Fig. 24.

$$\rho_{ij} = \frac{\left| \iint_{4\pi} [\mathbf{F}_i(\theta,\phi) \bullet \mathbf{F}_j^*(\theta,\phi)] d\Omega \right|^2}{\iint_{4\pi} |\mathbf{F}_i(\theta,\phi)|^2 \, d\Omega \iint_{4\pi} |\mathbf{F}_j(\theta,\phi)|^2 \, d\Omega} \quad (1)$$

where $\mathbf{F}_i(\theta, \varphi)$ is a complex vector indicating the vector field radiated from the ith element, and symbols • and * denote the Hermitian product and complex conjugate, respectively [2]. Similar to the *S*-parameters of the antenna system, $\rho_{21}=\rho_{32}=\rho_{43}=\rho_{41}$, and $\rho_{31}=\rho_{42}$. For brevity, only ρ_{21} and ρ_{31} are presented here. It can be seen that the ECC is always below 0.02 over the operating bandwidth, indicating the good MIMO performance of the proposed four-element antenna system.

V. Conclusion

The isolation enhancement of a closely-spaced four-element MIMO antenna system has been achieved by utilizing a crossed double-layer mushroom wall structure. For the parallel directed antenna element pairs, an isolation enhancement of 16 dB has been demonstrated such that the measured isolation between any element has been larger than 42 dB with a ground plane size of $0.96\lambda_0 \times 0.96\lambda_0$, and the calculated ECC has been lower than 0.02 within the operating band of 2.39 GHz–2.45 GHz. The results have shown that the proposed isolation enhancement technique can be applied to improve the performance of modern MIMO communication systems.

It should be noted that the utilization of the double-layer mushroom wall has not only reduced the transverse size, but also dramatically enhanced the inter-element isolation of the MIMO antenna system. However, the height of the antenna system increases to $0.17\lambda_0$, which may limit the antenna for some specific applications wherein the height of the antenna is critical. A low-profile MIMO antenna system with high inter-element isolation is desired for practical applications while challenging.

References

[1] A. Ghosh, R. Ratasuk, B. Mondal and N. Mangalvedhe, "LTE- advanced: next-generation wireless broadband technology," *IEEE Wireless Comm.*, vol. 17, no. 3, pp. 10–22, Jun. 2010.

[2] R. G. Vaughan and J. B. Andersen, "Antenna diversity in mobile communication," *IEEE Trans. Veh. Tech.*, vol.36, no.4, pp.149–170, Nov. 1987.

[3] S. Blanch, J. Romeu and I. Corbella, "Exact representation of antenna system diversity performance from input parameter description," *Electronic Lett.*, vol. 39, no. 9, pp. 705–707, May. 2003.

[4] R. Janaswamy, "Effect of element mutual coupling on the capacity of fixed length linear arrays," *IEEE Antennas Wireless Propag. Lett*., vol. 1, no. 1, pp. 157–160, 2002.

[5] G. J. Foschini and M. J. Gans, "On limit of wireless communications in a fading environment when using multiple antennas," *Wireless Personal Comm*., vol. 6, pp. 311–335.

[6] S. Farsi, H. Aliakbarian, D. Schreurs and B. Nauwelaers, "Mutual coupling reduction between planar antennas by using a simple microstrip U-section," *IEEE Antennas Wireless Propag. Lett*., vol. 11, pp. 1501–1503, 2012.

[7] H. L. Peng, , R. Tao, W. Y. Yin and J. F. Mao, "A novel compact dual-band antenna array with high isolations realized using the neutralization technique," *IEEE Trans. Antennas Propag*., vol. 61, no. 4, pp. 1958–1962, Apr. 2013.

[8] S. Zhang, S. N. Khan and S. L. He, "Reducing mutual coupling for an extremely closely-packed tunable dual-element PIFA array through a resonant slot antenna formed in-between," *IEEE Trans. Antennas Propag*., vol.58, no.8, pp.2771–2776, Aug. 2010.

[9] F. Yang and Y. R Samii, "Microstrip antennas integrated with electromagnetic band-gap (EBG) structures: a low mutual coupling design for array applications," *IEEE Trans. Antennas Propag*., vol. 10, no. 2, pp. 2936–2946, Feb. 2003.

[10] E. R.- Iglesias, O. Q-Teruel and L. I.-Sanchez, "Mutual coupling reduction in patch antenna arrays by using a planar EBG structure and a multilayer dielectric substrate," *IEEE Trans. Antennas Propag*., vol. 56, no. 6, pp. 1648–1655, Jun. 2008.

[11] L. Qiu, F. Zhao, K. Xiao, S. L. Chai and J. J. Mao, "Transmit-receiver isolation improvement of antenna arrays by using EBG strucuttres," *IEEE Antennas Wireless Propag. Lett*., vol. 11, 2012, pp.93–96.

[12] G. Dadashzadeh, A. Dadgarpour, F. Jolani and B.S. Virdee, "Mutual coupling suppression in closely spaced antennas," *Inst. Electr. Eng. Pro. Micro., Antennas Prpag*., vol. 5, no. 1, pp. 113–125, Jan. 2011.

[13] T.-I. Lee and Y. Wang, "Mode-based information channels in closely coupled dipole pairs," *IEEE Trans. Antennas Propag*., vol. 56, no. 12, pp. 3804–3811, Dec. 2008.

[14] J. C. Coetzee and Y. T. Yu, "Port decoupling for small arrays by means of an eigenmode feed network," *IEEE Trans. Antennas Propag*., vol. 56, no. 6, pp. 1587-1593, Jun. 2008.

[15] L.K. Yeung and Y. Wang, "Mode-based beamforming arrays for miniaturized platforms," *IEEE Trans. Antennas Propag*., vol. 57, no. 1, pp. 45–52, Jan. 2009.

[16] K. Wang K, L Li and T. F. Eibert, "Comparison of compact monopole antenna arrays with eigen mode excitation and multiport conjugate matching," *IEEE Trans. Antennas Propag*., vol. 61, no. 8, pp. 4054–4062, Aug. 2013.

[17] L. Y. Zhao and K. L. Wu, "A decoupling technique for four-element symmetric arrays with reactively loaded dummy elements," *IEEE Trans. Antennas Propag*., vol. 62, no. 8, pp. 4416–4421, Aug. 2014.

[18] R. R. Ramirez and F. D. Flaviis, "A mutual coupling study of linear and circular polarized microstrip antennas for diversity wireless systems," *IEEE Trans. Antennas Propag*., vol. 51, no. 2, pp. 5208–248, Feb. 2003.

[19] B. Wu and K. M. Luk, "A 4-port diversity antenna with high isolation for mobile communications," *IEEE Trans. Antennas Propag*., vol. 59, no. 5, pp. 1660–1667, May. 2011.

[20] A. A. Gheethan, P. A. Herzig and G. Mumcu, "Compact four-element coupled double Loop GPS antenna array loaded with broadside coupled split ring resonators," *IEEE Trans. Antennas Propag*., vol. 61, no. 6, pp. 3000–3008, Jun. 2013.

[21] D. K. Ntaikos and T. V. Yioultsis, "Compact split-ring resonator-loaded multiple-input–multiple-output antenna with electrically small elements and reduced mutual coupling," *Inst. Electr. Eng. Pro. Micro., Antennas Prpag.*, vol. 7, no. 6, pp. 421–429, Jun. 2013.

[22] M. S. Sharawi, M. U. Khan, A. B. Numan and D. N. Aloi, "A CSRR loaded MIMO antenna system for ISM band operation," *IEEE Trans. Antennas Propag*., vol. 61, no. 8, pp. 4265–4274, Aug. 2013.
[23] S. Ghosh, T. N. Tran and T. L-Ngoc, "Dual-layer EBG based miniaturized multi-element antenna for MIMO systems," *IEEE Trans. Antennas Propag*., vol. 62, no. 8, pp. 3985–3997, Aug. 2014
[24] H. Li, J. Xiong and S. L. He, "A compact planar MIMO antenna system of four elements with similar radiation characteristics and isolation structure," *IEEE Antennas Wireless Propag. Lett*., vol. 8, pp. 1107–1110, 2009
[25] G. H. Li, H. Q. Zhai, Z. H. Ma, C. H. Liang, R. D. Yu and S. Liu, "Isolation-improved dual-band MIMO antenna array for LTE/WiMAX mobile terminals," *IEEE Antennas Wireless Propag. Lett*., vol. 13, pp. 1128–1131, 2014.
[26] CST Microwave Studio, Computer Simulation Technology [Online]. Available: https://www.cst.com/Products/CSTMWS
[27] G. Q. Luo, Z. F. Hu, W. J. Li, X. H. Zhang, L. L. Sun and J. F. Zheng, "Bandwidth enhanced low profile cavity backed slot antenna by using hybrid SIW cavity modes," *IEEE Trans. Antennas Propag*., vol.60, no.4, pp.1698–1704, Apr. 2012.
[28] D. Sievenpiper, "High-impedance electromagnetic surface," Ph.D. desertion, Dept. Elect. Eng., Univ. California at Los Angeles, Los Angeles, CA, 1999
[29] Ansys HFSS, [Online]. Available: https:/www.ansys.com/Products/Simulation+Technology/Electronics/Signal+Integrity/ANSYS+HFSS

Guohua Zhai (M'15) was born in Shandong Province, China, in 1981. He received the B.Sng. degree from Qufu Normal University, Jining, China, in 2003, the M.Sng. degree in radio engineering from Nanjing Institute of Electronic Technology, Nanjing, China, in 2006, and the Ph.D. degree in radio engineering from Southeast University, Nanjing, China, in 2009.

Since September 2009, he has been with the faculty of East China Normal University as a Lecturer and later an Associate Professor. Since 2013, He is with the Institute for Infocomm Research (I^2R), Singapore. His current research interests include microwave and millimeter-wave passive devices, and MIMO antenna system.

Zhi Ning Chen (M'99–SM'05–F'07) received his B.Eng., M.Eng., and Ph.D. degrees, all in Electrical Engineering, from the Institute of Communications Engineering (ICE), Nanjing, China, and his second Ph.D. degree from University of Tsukuba, Ibaraki, Japan, respectively.

During 1988–1995, he worked at ICE as a Lecturer and later an Associate Professor, as well as at Southeast University, China, as a Postdoctoral Fellow and later as an Associate Professor. During 1995–1997, Dr. Chen joined the City University of Hong Kong as a Research Assistant and later a Research Fellow. In 1997, he was awarded the Japan Society for the Promotion of Science (JSPS) Fellowship to conduct his research at the University of Tsukuba, Japan. In 2001 and 2004, he visited the University of Tsukuba under a JSPS Fellowship Program (senior level). In 2004, he worked at IBM T. J. Watson Research Center, USA as an Academic Visitor. During 1999–2012, he worked with the Institute for Infocomm Research (I^2R) (formerly known as Centre for Wireless Communications and Institute for Communications Research) as Member of Technical Staff (MTS), Senior MTS, Principal MTS, Senior Scientist, Lead Scientist, and Principal Scientist as well as Head for RF & Optical Department. Since 2012, Dr. Chen joined the Department of Electrical and Computer Engineering, National University of Singapore as a Full Professor. He is concurrently holding a joint appointment as Advisor and Principle Scientist at I^2R as well as Visiting/Adjunct/Guest Professor positions at Southeast University, Nanjing University, Shanghai Jiaotong University, Tsinghua University, Tongji University, University of Science and Technology of China, Fudan University (Outstanding Overseas Professor), Dalian Maritime University, Chiba University, National Taiwan University of Science and Technology, Shanghai University (Ziqiang Professor) as well as City University of Hong Kong. During May-June 2013, he was a Senior DIGITEO Guest Scientist at the "Laboratoire des SignauxetSystèmes", UMR8506 CNRS-Supelec-University Paris Sud in Gif-sur-Yvette, France.

Dr. Chen has been the founding General Chairs of International Workshop on Antenna Technology (iWAT), International Symposium on InfoComm & Media Technology in Bio-Medical & Healthcare Applications (IS 3T-in-3A), International Microwave Forum (IMWF) as well as Asia-Pacific Conference on Antennas and Propagation (APCAP).

Dr. Chen's current research interest includes electromagnetic engineering, antennas for microwaves, mmW, submmW, and THz communication, radar, imaging and sensing systems. He has published 480 technical papers and authored/edited the books entitled *Broadband Planar Antennas* (Wiley 2005), *UWB Wireless Communication* (Wiley 2006), *Antennas for Portable Devices* (Wiley 2007), and *Antennas for Base Stations in Wireless Communications* (McGraw-Hill 2009). He also contributed to the books entitled *UWB Antennas and Propagation for Communications, Radar, and Imaging* (Wiley 2006), *Antenna Engineering Handbook* (McGraw-Hill 2007) as well as *Microstrip and Printed Antennas* (Wiley 2010). He is holding 30 granted and filed patents with 31 licensed deals with industry. He is the recipient of International Symposium on Antennas and Propagation Best Paper Award 2010, the CST University Publication Award 2008, IEEE AP-S Honorable Mention Student Paper Contest 2008, IES (Institution of Engineers Singapore) Prestigious Engineering Achievement Awards 2006, 2013 and 2014, Singapore Manufacturing Federation Award 2014, I^2R Quarterly Best Paper Award 2004, and IEEE iWAT 2005 Best Poster Award.

Dr. Chen is a Fellow of the IEEE *for the contribution to small and broadband antennas for wireless applications*. He is serving IEEE Trans Antennas and Propagation as an Associate Editor and served IEEE Antennas and Propagation Society as a Distinguished Lecturer during 2009–2011.

Xianming QING (M'90-SM'15) received the B.Eng. degree from University of Electronic Science and Technology of China (UESTC), Chengdu, China, in 1985, and the Ph.D. degree from Chiba University, Chiba, Japan, in 2010.

During 1987–1996, Dr. Qing was with UESTC for teaching and research and appointed as a Lecturer in 1990 and an Associate Professor in 1995. He joined National University of Singapore (NUS) in 1997 as a Research Scientist. Since 1998, he has been with the Institute for Infocomm Research (I^2R, formerly known as CWC and ICR), Singapore. He is currently holding the position of Senior Scientist and Head of Antenna System Laboratory. His main research interests are antenna design and characterization for wireless applications. In particular, his current R&D focuses on small and broadband antennas/arrays for wireless systems, such as ultra-wideband (UWB), radio frequency identification (RFID), medical imaging, and microwave, mmW, submmW, and THz imaging systems.

Dr. Qing has authored and co-authored over 190 technical papers published in international journals or presented at international conferences, and 5 book chapters. He is holding 10 granted and filed patents. He received six Advancement of Science and Technology Awards, in P. R. China from 1987 to 1997. He is also the recipient of the IES (Institution of Engineers Singapore) Prestigious Engineering Achievement Awards 2006, 2013 and 2014; Singapore Manufacturing Federation Award 2014, and the ISAP Best Paper Award 2010.

Dr. Qing has been a member of the IEEE Antennas and Propagation Society since 1990. He has severed the member for the RFID Technical Committee (TC-24) of the IEEE MTT since 2009. He severed the organizer and chair for special sessions on RFID antennas at IEEE Antenna and Propagation Symposium 2007 and 2008. He is serving as the associate editor of the *International Journal of Microwave and Wireless Technologies* (Cambridge University Press/EuMA) and *International Journal of Microwave Science and Technology*, *International Journal of Antennas and Propagation* (Hindawi Publishing Corporation). He also served the guest editor of the special issue "Antennas for Emerging Radio Frequency Identification (RFID) Applications" at *International Journal on Wireless & Optical Communications*. He has served as the TPC member and session chair for a number of conferences, and the regular reviewer for *IEEE T-AP, T-MTT, IEEE-AWPL, MWCL, IET-MAP, Electronic Letters*, etc.